

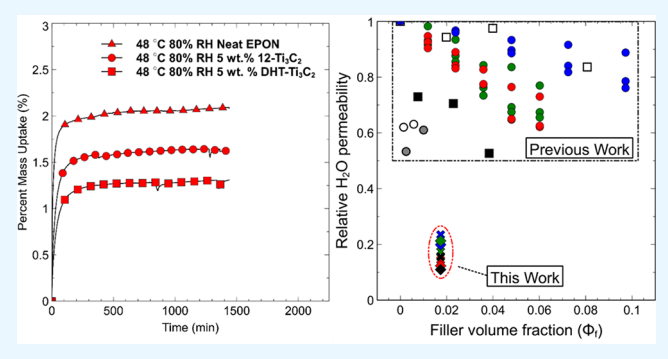
Water Transport and Thermomechanical Properties of Ti₃C₂T_z MXene Epoxy Nanocomposites

Michael S. Carey, Maxim Sokol, Giuseppe R. Palmese, and Michel W. Barsoum*,

[†]Department of Materials Science and Engineering and [‡]Department of Chemical and Biological Engineering, Drexel University, Philadelphia, Pennsylvania 19104, United States

Supporting Information

ABSTRACT: Herein, we present the fabrication of dispersed, 5.0 wt % (1.74 vol %) ${\rm Ti_3C_2T_z}$ MXene epoxy nanocomposites (NCs), and report on their water transport and mechanical properties. To make the composites, Li⁺ ions between ${\rm Ti_3C_2T_z}$ MXene multilayers, MLs, present after the etching step were exchanged with either 12-aminolauric acid, ALA, or di-(hydrogenated tallow)benzyl methyl ammonium chloride, DHT. After drying, the resulting ML powders were added at room temperature to the epoxy resin (diglycidyl ether of bisphenol A), followed by the curing agent, triethylenetetramine. The NCs were characterized by X-ray diffraction, thermogravimetric analysis, dynamic vapor sorption, dynamic



mechanical analysis, scanning and transmission electron microscopies, and infrared spectroscopy. From XRD, the lack of signature MXene basal peaks, as well as evidence of exfoliation supported by TEM micrographs, we conclude that the MXene ML had indeed been intercalated by the epoxy. The distribution of the exfoliated multilayers, MLs, however, was not uniform. Nevertheless, our relative permeabilities, with a 1.74 vol % loading, are 5 times lower than results obtained in the carbon- or clay-reinforced epoxy NC literature. The lower permeabilities are due to reductions in both solubilities and diffusivities relative to the neat polymer. In the case of DHT, the water solubility at all temperatures was almost halved. The mechanical properties and thermal stability are found to be slightly improved with the addition of DHT-MXene. As far as we are aware, this is the first report of exfoliation of MXene in an epoxy matrix. Additionally, this study is the first to measure the diffusion of water in MXene epoxy NCs. More work on better dispersion of the MLs is indicated and ongoing.

KEYWORDS: MXene, polymer, nanocomposite, epoxy, barrier properties

1. INTRODUCTION

Epoxies are a class of thermosetting polymers that find use in many applications, ranging from coatings, adhesives, and structural parts to hybrid materials, and they are widely used as the predominant component of composites. The resins used in epoxies are composed of functional groups with threemembered cyclic ether rings known as epoxides, shown in Figure 1a. Being highly strained, this epoxide ring is rather reactive, particularly with amines, aminoamides, and phenolic compounds (among others). The reaction with these agents results in the epoxide ring opening and polymerizing to form a network thermoset. In addition to wide use as coatings and adhesives, epoxies are often used to encapsulate electronic components and protect metal substrates from oxidation. Therefore, it is vitally important that their resistance to moisture is maximized to prevent delamination or degradation.^{1,2} As importantly, absorbed water can detrimentally affect the thermal and mechanical properties of epoxy resins, as well as initiate corrosion, in the case of metallic substrates.

Inspired by the Toyota researchers who pioneered the development of nylon-6-based nanocomposites, NCs, Wang and Pinnavaia demonstrated that montmorillonite (MMT), a

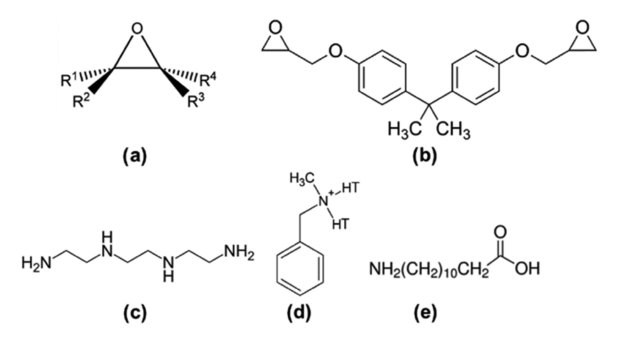


Figure 1. Chemical structures of (a) epoxide functional group, (b) bisphenol A diglycidyl ether, (c) triethylenetetramine, (d) di-(hydrogenated tallow)benzyl methyl ammonium chloride (HT = hydrogenated tallow, C_{16} – C_{18}), and (e) 12-aminolauric acid.

2:1 layered silicate, can be dispersed into diglycidyl ether of bisphenol A (DGEBA) by its treatment with acidic onium ions

Received: June 30, 2019 Accepted: September 20, 2019 Published: September 20, 2019 such as $[H_3N(CH_2)_{n-1}COOH]^+$, $[H_3N(CH_2)_nNH_2]^+$, $[H_3N-1]^+$ $(CH_2)_nNH_3$, or $[H_3N(CH_2)_{n-1}CH_3]^+$, with n=6 or 12.⁴ This work has been expanded upon, and to date, many authors have dispersed clays in epoxy resins and studied the resulting properties.5-12

Among many other improvements in material properties, clay polymer NCs exhibit excellent resistance to the permeation of gases and moisture. Permeability generally decreases as the volume fraction of nanofiller, $\phi_{\rm fr}$ is increased and ascribed to a longer path with greater tortuosity that a diffusing species must navigate to permeate a membrane. 13-16

Assuming uniformly distributed platelets that are all oriented normal to the direction of diffusion, Nielsen quantitatively described the relative permeability, R, as

$$R = \frac{P_{\rm f}}{P_{\rm u}} = \frac{1 - \phi_{\rm f}}{1 + \frac{L\phi_{\rm f}}{2\Delta}} \tag{1}$$

where P_{c} , P_{w} , L, and Δ are the permeability of the composite, permeability of the polymer, platelet thickness, and lateral flake size, respectively. 17 Nielsen's model and those developed since share the common feature of the dependence of R on L/Δ and $\phi_{\rm f}$ where increases in $\phi_{\rm f}$ and/or L/Δ , result in a decrease in

Water vapor transport can be modeled by measuring mass uptake in thin films. From this model, the diffusion coefficient, D, of water can be calculated from plots of the mass at time $(M_{\rm t})$, relative to the mass at equilibrium $(M_{\rm eq})$ versus the square root of t. Since that ratio is given by t

$$\frac{M_{\rm t}}{M_{\rm eq}} = \frac{4}{d} \sqrt{\frac{Dt}{\pi}} \tag{2}$$

where d is the film thickness. The sample's permeability, P, is therefore given by

$$P = D \cdot S \tag{3}$$

where S is the solubility. ¹⁹ The ratio of P_c/P_u gives the relative permeability, and R can then be described simply as

$$R = \frac{P_{\rm c}}{P_{\rm u}} \tag{4}$$

Discovered in 2011, MXenes (pronounced MAX-enes) are among the most recently discovered 2D materials.²⁰ MXenes are derived from the machinable, nanolaminated ternary carbides and nitrides known as MAX phases, which have the formula $M_{n+1}AX_n$, in which M, A, and X represent distinct layers, and n ranges from 1 to 3. Specifically, M is an early transition metal, such as Ti, A is an A-group element, such as Al, and X is C and/or N. These MAX phases are composed of layers of pure A separating M_{n+1}X_n layers.²¹ Through the selective etching of the A-group element (typically Al), the 3D parent MAX phase is converted to a 2D MXene. For further details regarding MAX phases, as well as MXenes and their synthesis, we direct the reader to more comprehensive reviews. 22,23

Interestingly, MXenes share many common features with clays. For example, both MXenes and clays form stable colloidal suspensions in water around pH \sim 7, have similar interlayer spaces that contain exchangeable cations and/or water, and the spacing of the interlayer space is a function of the intercalated species, as well as relative humidity.²⁴⁻²⁷ Given the prominent success of clay polymer composites, and

the demonstrated similarities between clays and MXenes, we recently reported on the full dispersion of Ti₃C₂T₂ MXene in nylon-6 by first treating MXene multilayers (MLs) with 12aminolauric acid (ALA) (Figure 1e). The resulting NCs showed record low water vapor barrier properties for nylonreinforced NCs.²⁸ The work presented herein builds upon our nylon work, as we set out to disperse Ti₃C₂T_z in DGEBA resin, cured with triethylenetetramine (TETA).

This work aims to study the barrier properties of the resulting NCs to permeating water vapor. This was achieved by changing the nature of the intergallery space from hydrophilic to hydrophobic by ion-exchanging the Li ions present between the MLs with di(hydrogenated tallow)benzyl methyl ammonium chloride (DHTBMA) or ALA. The best results were obtained by the treatment with the former. For brevity's sake, henceforth, DHTBMA will be referred to as DHT.

2. RESULTS AND DISCUSSION

The MXene loading in the NCs was verified by thermogravimetric analysis. Figure 2 shows that the residual mass, after

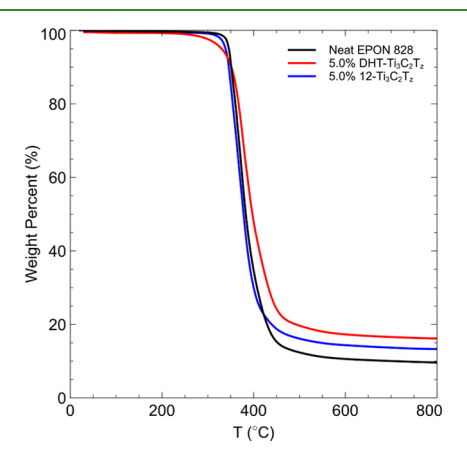


Figure 2. TGA curves of weight loss of neat epoxy and 5 wt % DHT- $Ti_3C_2T_z$ NC.

subtracting the char yield, is close to the targeted MXene loading of 5 wt %, which was chosen based on our previous results on MXene nylon-6 nanocomposites.²⁸ Note that the degradation temperature is slightly increased in the DHT-MX NC. Such enhancements in thermal stability have been observed before and have been linked to enhanced barrier qualities, as volatile decomposition products must take a torturous path out of the material. 10,29-31

The XRD results indicate that the basal spacing of untreated Ti₃C₂T_z (Figure 3a), nominally 14.6 Å, increased when treated with ALA (Figure 3b), forming separate peaks at basal spacings of 15.8 and 20.2 Å. (The basal spacings, equal to half the clattice parameter determined for the 0002 peaks, can be read off the top y-axis.) The treatment with DHT (Figure 3c), on the other hand, resulted in a drastic increase of the basal spacing to 39.0 Å. The smaller, higher angle peaks at 4.6 and 7.1° are reflections of higher order peaks. Most importantly, there is a total absence of any peak in the DHT-MX NC (Figure 3e). In the ALA-MX NC (Figure 3d) case, a broad peak of around 6.45° is observed. This peak can likely be attributed to partially intercalated MLs. The results shown in Figure 3e cannot be overemphasized since they strongly suggest that, like in other NC systems, exfoliation of the MLs has been achieved. This exfoliation has been repeatedly shown

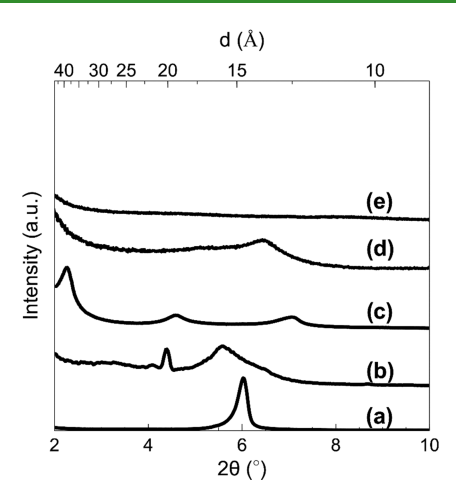


Figure 3. X-ray diffractograms of Ti₃C₂T_z MLs and NCs. (a) Asetched MXene MLs, (b) ALA-MX MLs, (c) DHT-MX MLs, (d) ALA-MX NC, and (e) DHT-MX NC.

to be the key factor responsible for the enhancements in the properties of polymeric NCs, including thermal stability, mechanical reinforcement, and enhanced barrier resistance. 12,32

While the XRD results indicate that no basal ordering remains, based on the TEM micrograph presented in Figure 4,

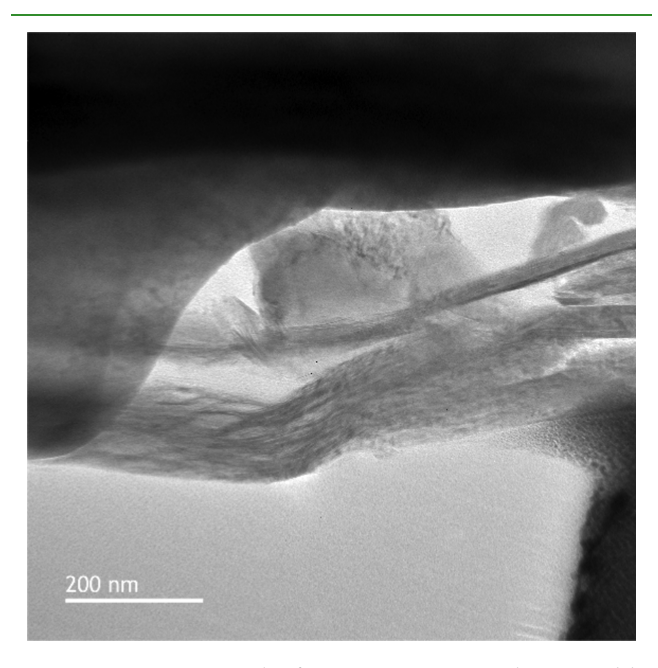


Figure 4. TEM micrograph of a 5 wt % DHT sample prepared by focused ion beam milling.

it would appear that indeed some dispersion of flakes has occurred; however, some few-flake stacks remain. Finding a region that contained MXene flakes in the TEM was a challenge; most areas did not contain MXenes. This somewhat surprising result was only understood when Ti EDS maps on fractured surfaces were acquired (Figure 5). It is obvious that the dispersion of the Ti₃C₂T_z flakes was not uniform at the scale shown in Figure 5a,b. The Ti-rich clusters are most probably single, or few, ML particles that result from the etching stage (Figure 5c). The accordion-like morphology is typical of postetched Ti₃AlC₂ (i.e., Ti₃C₂) particles. This

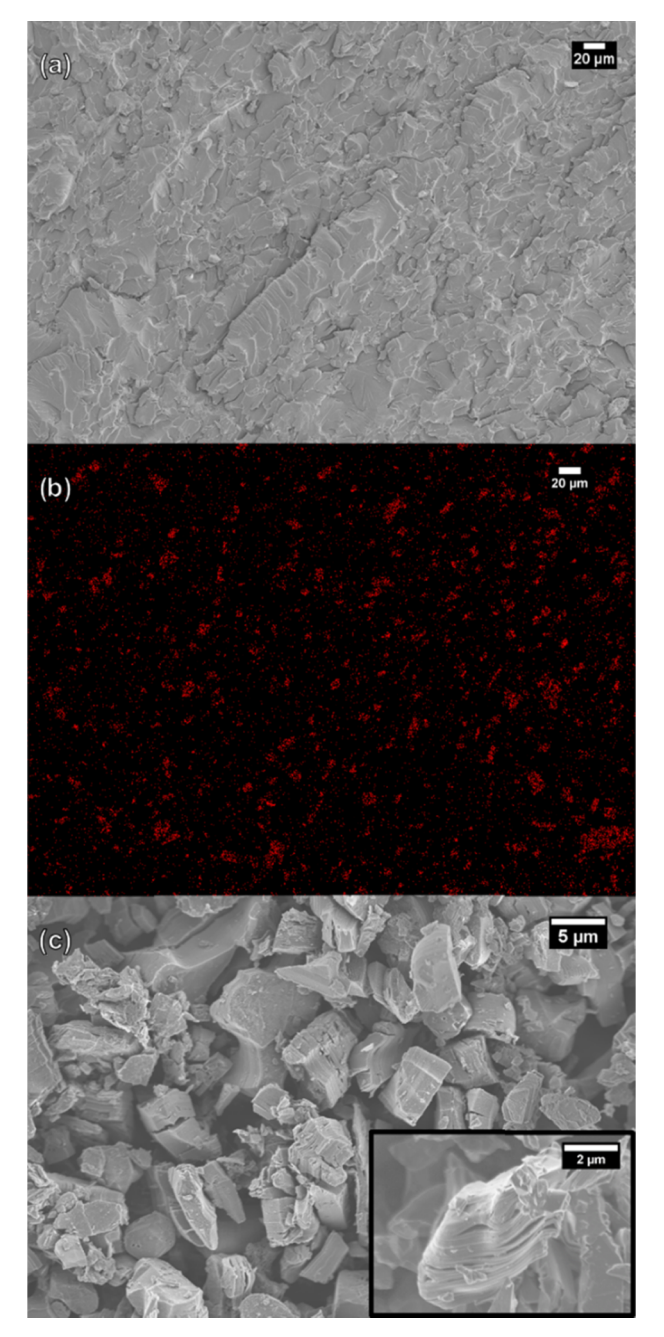


Figure 5. (a) SEM image of DHT-MX NC tensile fracture surface and (b) Ti EDS map of the same. (c) Typical SEM micrograph of ML particles after DHT treatment. Inset shows a higher magnification of a single particle.

comment notwithstanding, it is important to point out that the MLs are indeed dispersed at the TEM level (Figure 4) as evidenced by the fact that the polymer has penetrated between all of the flakes regardless of how tightly spaced they are. It follows that more work, some of which is currently ongoing, is necessary to improve the degree of dispersion at the SEM level. It is not unreasonable to assume that the application of shear stresses during mixing and/or mixing at higher temperatures would better disperse the MLs.

Exfoliation is generally attributed to the intercalation of either resin or hardener into the interlayer space of an organoclay. The mechanism of exfoliation is described by the difference in kinetics between the inner and outer layer spaces.

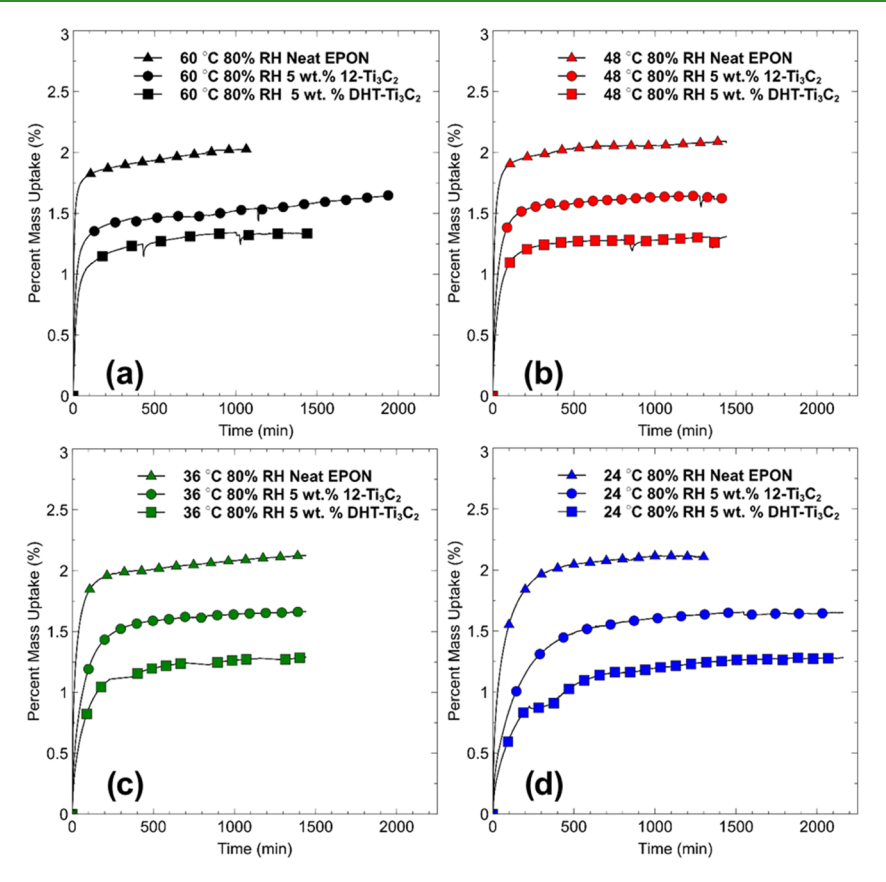


Figure 6. Time dependence of mass for neat (triangles), ALA-MX (circles), and DHT-MX (squares) NCs held at 80% RH, and (a) 60 °C, (b) 48 °C, (c) 36 °C, and (d) 24 °C.

As the curing agent is introduced, the surface agents used to make the clay organophilic promote the reaction between intercalated monomer with the chemical hardener, thereby speeding up the curing reaction in the interlayer space, relative to the curing reaction outside the galleries. This disparity in reaction kinetics facilitates exfoliation of clay sheets by separating the layers. By utilizing MXene rather than layered silicates, this mechanism allows for the in situ polymerization reaction to occur and an exfoliated MXene composite to be obtained, as shown in Figure 4.

Figure 6a-d plots the percent mass uptake as a function of time, measured by dynamic vapor sorption (DVS) analysis of neat, ALA-, and DHT-MX NC thin films at the tested temperatures of 60, 48, 36, and 24 °C at an 80% relative humidity (RH), respectively. In all figures, and throughout this paper, all of the neat epoxy results are plotted as triangles, the ALA-MX results as circles, and the DHT-MX results as squares. From these results, it is obvious that at all temperatures the equilibrium water solubility, S, decreases as one goes from the neat to the DHT-MX samples, with the latter having the lowest solubility. Additionally, across all specimens, *S* is weakly dependent on temperature (Figure S2). Figure S1a-d replots the normalized mass uptake, M_t/M_{eq} vs $t^{1/2}$. The initial region, where linear uptake is observed, can be used to extract the diffusion coefficient, according to eq 2. Like S, the diffusivity, D, is highest in the neat epoxy films and significantly reduced in the NCs. However, unlike S, D varies with temperature, as the Arrhenius plot of D, Figure 7,

This reduction in D is typically attributed to the more tortuous path a diffusing water molecule must take around the

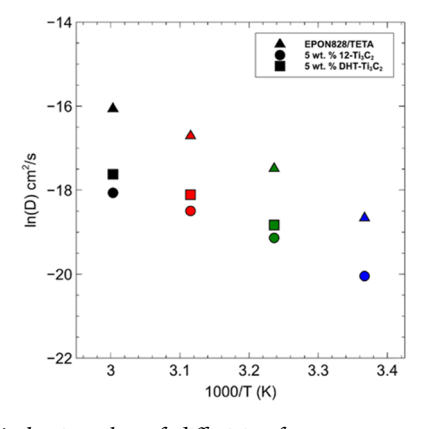


Figure 7. Arrhenius plot of diffusivity for neat epoxy (triangles), DHTBMA-MX (squares), and ALA-MX (circles) samples.

high-aspect-ratio nanofiller, as first described by Nielsen and embodied by eq $1.^{17}$ However, based on the microstructure shown in Figure 5, it is not clear how much effect tortuosity would have on D. It is hereby acknowledged that what causes the clear and unambiguous reduction in D is unclear. The affinity for water to populate the interlayer space of MXene stacks cannot be ruled out and requires further study. 27,36,37

The permeability, P, of the films can be calculated from eq 4 and the experimentally obtained values of S and D. By taking the ratio of P of the filled and unfilled samples, R can be calculated. Figure S3 plots R vs filler volume fraction together with those determined for other epoxy/clay, $^{8,9,38}_{,9,38}$ epoxy/carbon nanotube, $^{6,39}_{,9,39}$ and epoxy nanofiber $^{39}_{,9,39}$ studies. Also plotted are Nielsen's equation (eq 1) for various aspect ratios. Based on

this figure, one could conclude that the aspect ratio of our dispersion is about 1000, a conclusion belied by Figure 5. It follows that before any meaningful conclusions can be reached based on eq 1, the microstructure needs to confirm the presence of a uniform dispersion.

The thermomechanical properties of the neat epoxy and NCs were investigated by DMA, from which the storage, E', and loss moduli, E'', were calculated. The results are plotted in Figure 8. The glass-transition temperature, T_g , is obtained from

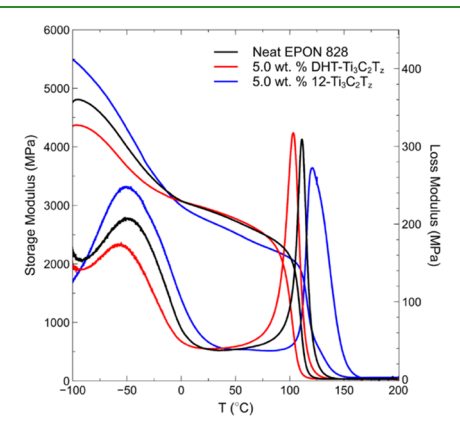


Figure 8. Storage and loss modulus of neat epoxy, DHT-MX, and ALA-MX NCs.

 $\tan \delta$ vs temperature plots (Figure S4). Note that at room temperature, the DHT-MX samples have slightly higher storage moduli (E') and a lower $T_{\rm g}$ than the neat samples.

This limited improvement in mechanical properties is likely due to a lack of exfoliation of the MX MLs in the ALA-MX NCs and the partial exfoliation in DHT-MX NCs (Figures 4 and 5). Nevertheless, our results are in agreement with the clay/epoxy NC literature, as the predominant failure mode of glassy polymers is crack propagation, initiated by crazing and caviation. 40 Nanofillers struggle to impede this crack propagation, even in fully dispersed systems, as there is little platelet alignment along the direction of applied strain. In rubbery or viscoelastic polymers, the strain-induced alignment results in far superior improvements in mechanical properties.⁵

Thin neat and NC sample films used for DVS were also studied by FTIR-ATR in both the hydrated (Figure 9a) and dry states (Figure 9b). The broad shoulder centered around 3400 cm⁻¹ corresponds to hydrogen-bonded NH bending and stretching modes. It is clear that the NC samples have weak shoulders in the region in both the dry and saturated states, while the neat epoxy films have more pronounced bands, particularly in the saturated state. Additionally, the shoulder of the ALA-MX-treated sample is stronger than that of DHT-MX, suggesting a larger degree of bound water in the former, which agrees well with DVS results where ALA-treated samples had higher water solubility than those treated by DHT.

3. CONCLUSIONS

Herein, we report Ti₃C₂T_z MXene epoxy NCs, loaded with 5.0 wt % (1.74 vol %) Ti₃C₂T_z MXene flakes. Cations present between the Ti₃C₂T_z MLs after the etching stage were exchanged with ALA or DHT before gentle mixing with diglycidyl ether of bisphenol A (EPON-828) epoxy resin and curing agent, triethylenetetramine (EPIKURE 3234) to initiate the curing reaction in the presence of intercalated, organophilic Ti₃C₂T_z, resulting in exfoliated MXene epoxy NCs. This is

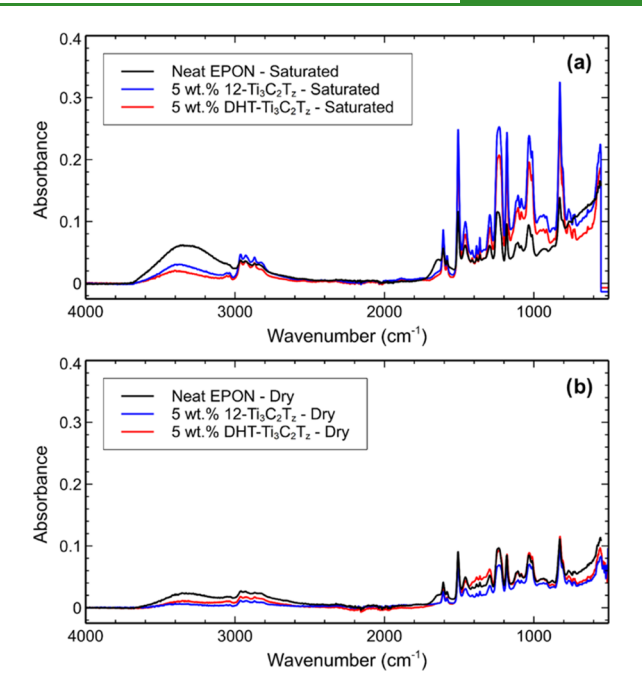


Figure 9. FTIR-ATR spectra of neat, ALA-MX, and DHT-MX NC thin films in the (a) water-saturated state and (b) dry state.

supported by the absence of MXene basal peaks in our 5.0 wt % DHT-treated MXene and TEM micrographs. The dispersion of the epoxy-infused MLs, however, was not uniform. Nevertheless, comparison of our relative permeabilities with others in the literature of similar NCs indicates that our values are remarkably low. Additionally, the equilibrium solubility of water is uniformly lowered in NC samples. The relative permeability of the epoxy resin was reduced by up to 90% with a loading of only 5 wt % (1.74 vol %) Ti₃C₂T_z.

As far as we are aware, this is the first report of MXene exfoliation in epoxy, as well as the first report on water diffusion in MXene/epoxy composites.

Finally, we note that the challenge of dispersing the MLs in the polymer matrix has been overcome. This was by the organophilic modification of MXene using ALA or, better, DHT. We are currently working on the additional challenge of better dispersing the ML clusters.

4. EXPERIMENTAL SECTION

4.1. Synthesis of Ti₃AlC₂ and Ti₃C₂T_z. 4.1.1. Materials. Ti₃AlC₂ was made with powders of Ti, Al, and TiC (-325 mesh, 99.5%, Alfa Aesar, Ward Hill, MA). The epoxy resin EPON-828, a diglycidyl ether of bisphenol A (DGEBA) resin, and curing agent, EPIKURE 3234 (triethylenetetramine (TETA)) were commercially obtained (Miller Stephenson, Danbury, CT). The 12-ALA (>98.0%, TCI America, Portland, OR) and DHTBMAC (80%, Alfa Chemistry, Ronkonkoma, NY) were used for treatment of the $Ti_3C_2T_z$ MLs.

4.1.2. Ti₃AlC₂ Synthesis. Ti₃AlC₂ was synthesized as previously reported.²⁸

4.1.3. $Ti_3C_2T_2$ Synthesis and Treatment. Three grams of sieved MAX powder ($<38 \mu m$) were immersed in a 30 mL solution of 10 wt % hydrofluoric acid and 3.24 g lithium chloride for a LiCl/Ti₃AlC₂ molar ratio of 5:1. This mixture was stirred for 24 h with a poly(tetrafluoroethylene) (PTFE)-coated magnetic stir bar at RT at 300 rpm. After etching, the contents were equally divided into six centrifuge tubes so that the mass of each tube was within ± 0.01 g of the others. To obtain 1 g of untreated MXene and 1 g of each treatment, out of the six tubes, two were left untreated, two were treated with ALA, and two with DHT.

These tubes were centrifuged at 3500 rpm (or 2301 rcf) for 2 min to separate the sediment. The supernatant was discarded and each vial was refilled with 40 mL deionized water before another round of centrifugation. This washing procedure was repeated until the measured pH was around 5-6.

After the final wash, 40 mL of 20 mM preprepared solutions of ALA or DHT were added to the appropriately isolated sediments composed of multilayers—and allowed to mix for 12 h at RT. In the preparation of the ALA solution, 1.2 mL of 12 M HCl was added. After mixing, all powders were washed simultaneously with distilled water until aliquots added to a 1 M AgNO₃ solution indicated no signs of chlorine. The product was then vacuum-filtered through a porous polypropylene film (Celgard LLC, Charlotte, NC) and dried at 100 °C under vacuum for 12 h. The resulting fine powders are hereafter referred to as 12-MX or DHT-MX or simply MXene in the case of untreated powders.

- 4.2. Preparation and Synthesis of Neat and Composite Samples. Dried MXene powder of 1.05 g was added to 17.5 g of EPON-828 at a loading of 5 wt % in the final product, and the mixture was placed on a vortex mixer for 5 min before mixing on an orbital shaker for 12 h. The mixture was degassed for 10 min under vacuum before the addition of 2.45 g of TETA, followed by gentle handmixing for 5 min. The mixture was further degassed for an additional 0.5 h before pouring into predried silicone tensile and DMA molds. Thin films for DVS were prepared by drawing a small amount of the mixture down with a 100 μ m bird applicator onto a polyvinylflouridecoated steel panel. Samples were allowed to gel for 4 days, before postcuring at 100 °C for 12 h.
- **4.3.** Characterization Methods. 4.3.1. Thermogravimetric Analysis. The $Ti_3C_2T_z$ content was measured by thermogravimetric analysis, TGA (TA Instruments Q50, New Castle, DE). The samples were heated at a rate of 10 °C min⁻¹ to 800 °C under a 10 mL min⁻¹ Ar flow. To verify the final mass, the sample was held at 800 °C for 0.5 h.
- 4.3.2. X-ray Diffraction Analysis. X-ray diffraction, XRD, patterns were obtained using a Rigaku SmartLab X-ray diffractometer (Rigaku, Tokyo, Japan) with an incident Cu Kα wavelength of 1.54 Å in a stepwise mode from 2 to 10° with a step size of 0.02° and a dwell time of 1.5 s per step.
- 4.3.3. Dynamic Vapor Sorption Analysis. A dynamic vapor sorption, DVS, analyzer (TA Instruments Q5000SA, New Castle, DE) was used to study water permeation. Samples were dried at 80 °C and 0% RH for 12 h or until the mass change was less than 0.1%. After drying, the samples were tested isothermally at 60, 48, 36, or 24 °C, and 80% relative humidity while continuously measuring the sample mass. All films had a thickness of approximately 150 \pm 5 μ m.
- 4.3.4. Dynamic Mechanical Analysis. A dynamic mechanical analyzer (TA Instruments Q800, New Castle, DE) was utilized to measure the thermomechanical properties of rectangular bulk samples at 1 Hz and an amplitude of 10 μ m in a single cantilever mode from -100 to 200 °C at a rate of 2 °C min⁻¹. By casting into silicone molds, followed by careful hand-polishing, the samples were shaped into rectangular slabs 17.5 mm long, 12.7 mm wide, and 3 mm thick to give a span to thickness ratio >10. This ensures the accuracy of the measured glassy moduli, as well as keeping the rubbery data within the sensitivity limits of the instrument.⁴
- 4.3.5. Tensile Measurements. Tensile specimens were tested according to ASTM D638-14 in the type IV geometry. Uniaxial tensile measurements were performed on an Instron 8800 with a strain gauge attached to the samples and a 1 kN load cell with a 1 mm s-1 crosshead speed, for a nominal strain rate of 0.04 s⁻¹
- 4.3.6. FTIR-ATR Study. Mid-infrared, IR, spectra of thin samples were collected with a spectrometer (Thermo Fisher Nicolet Nexus 870 FTIR Spectrometer, Waltham, MA) in the range of 4000-400 cm⁻¹ at RT. For each sample, 32 scans were taken successively with a scan average of 4 (data spacing of 0.482 cm⁻¹). Dry samples were prepared by drying in vacuum at 100 °C for 12 h and storing under vacuum. After taking measurements on the dry films, they were placed in sealed containers of DI water and kept in a cool, dark drawer for 120 h. Water on the surface of samples was gently wiped with

KimTech wipes (Kimberly Clark, Irving, TX) before measuring the IR

4.3.7. Transmission Electron Microscopy and Focused Ion Beam. Transmission electron microscope (TEM) samples of a DHT-MX NC were prepared by a dual-beam focused ion beam (FIB), SEM (FEI Strata DB235). TEM images were taken using a JEOL JEM2100 transmission electron microscope operated at 200 kV.

ASSOCIATED CONTENT

Supporting Information

The Supporting Information is available free of charge on the ACS Publications website at DOI: 10.1021/acsami.9b11448.

Plots of normalized mass uptake vs square root of time to calculate diffusion coefficients for neat and nanocomposite films as a function of temperature at 80% RH; Arrhenius plot of solubility for neat and nanocomposite samples; Nielsen plot of relative H₂O permeability vs filler volume fraction; and plot of $tan(\delta)$ for neat and nanocomposite samples (PDF)

AUTHOR INFORMATION

Corresponding Author

*E-mail: barsoumw@drexel.edu.

ORCID ®

Michel W. Barsoum: 0000-0001-7800-3517

Author Contributions

The manuscript was written through contributions of all authors. All authors have given approval to the final version of the manuscript.

Funding

This work was supported by the National Science Foundation (DMR-1740795).

Notes

The authors declare no competing financial interest.

ACKNOWLEDGMENTS

The authors would like to thank Varun Natu for his assistance with SEM analysis and EDS mapping of the sample fracture

REFERENCES

- (1) Dušek, K.; Bell, J. P. Epoxy Resins and Composites II; Springer-Verlag, 1986.
- (2) Lupinski, J. H.; Moore, R. S.; et al. Polymeric Materials for Electronics Packaging and Interconnection; American Chemical Society,
- (3) Zhang, S.-Y.; Ding, Y.-F.; Li, S.-J.; Luo, X.-W.; Zhou, W.-F. Effect of Polymeric Structure on the Corrosion Protection of Epoxy Coatings. Corros. Sci. 2002, 44, 861-869.
- (4) Wang, M. S.; Pinnavaia, T. J. Clay-Polymer Nanocomposites Formed from Acidic Derivatives of Montmorillonite and an Epoxy Resin. Chem. Mater. 1994, 6, 468-474.
- (5) Lan, T.; Pinnavaia, T. J. Clay-Reinforced Epoxy Nanocomposites. Chem. Mater. 1994, 6, 2216-2219.
- (6) Starkova, O.; Buschhorn, S. T.; Mannov, E.; Schulte, K.; Aniskevich, A. Water Transport in Epoxy/MWCNT Composites. Eur. Polym. J. 2013, 49, 2138-2148.
- (7) Liu, W.; Hoa, S. V.; Pugh, M. Organoclay-Modified High Performance Epoxy Nanocomposites. Compos. Sci. Technol. 2005, 65,
- (8) Liu, W.; Hoa, S. V.; Pugh, M. Fracture Toughness and Water Uptake of High-Performance Epoxy/Nanoclay Nanocomposites. Compos. Sci. Technol. 2005, 65, 2364-2373.

- (9) Alamri, H.; Low, I. M. Effect of Water Absorption on the Mechanical Properties of Nano-Filler Reinforced Epoxy Nano-composites. *Mater. Des.* **2012**, *42*, 214–222.
- (10) Park, S.-J.; Seo, D.-I.; Lee, J.-R. Surface Modification of Montmorillonite on Surface Acid-Base Characteristics of Clay and Thermal Stability of Epoxy/Clay Nanocomposites. *J. Colloid Interface Sci.* **2002**, *251*, 160–165.
- (11) Kim, J.-K.; Hu, C.; Woo, R. S. C.; Sham, M.-L. Moisture Barrier Characteristics of Organoclay–Epoxy Nanocomposites. *Compos. Sci. Technol.* **2005**, *65*, 805–813.
- (12) Azeez, A. A.; Rhee, K. Y.; Park, S. J.; Hui, D. Epoxy Clay Nanocomposites–Processing, Properties and Applications: A Review. *Composites, Part B* **2013**, *45*, 308–320.
- (13) Alix, S.; Follain, N.; Tenn, N.; Alexandre, B.; Bourbigot, S.; Soulestin, J.; Marais, S. Effect of Highly Exfoliated and Oriented Organoclays on the Barrier Properties of Polyamide 6 Based Nanocomposites. J. Phys. Chem. C 2012, 116, 4937–4947.
- (14) Picard, E.; Vermogen, A.; Gérard, J.-F.; Espuche, E. Barrier Properties of Nylon 6-Montmorillonite Nanocomposite Membranes Prepared by Melt Blending: Influence of the Clay Content and Dispersion State: Consequences on Modelling. *J. Membr. Sci.* **2007**, 292, 133–144.
- (15) Picard, E.; Gérard, J.-F.; Espuche, E. Water Transport Properties of Polyamide 6 Based Nanocomposites Prepared by Melt Blending: On the Importance of the Clay Dispersion State on the Water Transport Properties at High Water Activity. *J. Membr. Sci.* **2008**, 313, 284–295.
- (16) Choudalakis, G.; Gotsis, A. D. Permeability of Polymer/Clay Nanocomposites: A Review. Eur. Polym. J. 2009, 45, 967–984.
- (17) Nielsen, L. E. Models for the Permeability of Filled Polymer Systems. J. Macromol. Sci., Part A 1967, 1, 929–942.
- (18) Crank, J.; et al. The Mathematics of Diffusion; Oxford University Press. 1979.
- (19) Hauser, P. M.; McLaren, A. D. Permeation through and Sorption of Water Vapor by High Polymers. *Ind. Eng. Chem.* **1948**, *40*, 112–117.
- (20) Naguib, M.; Kurtoglu, M.; Presser, V.; Lu, J.; Niu, J.; Heon, M.; Hultman, L.; Gogotsi, Y.; Barsoum, M. W. Two-Dimensional Nanocrystals Produced by Exfoliation of Ti₃AlC₂. *Adv. Mater.* **2011**, 23, 4248–4253.
- (21) Barsoum, M. W. MAX Phases: Properties of Machinable Ternary Carbides and Nitrides; John Wiley & Sons, 2013.
- (22) Sokol, M.; Natu, V.; Kota, S.; Barsoum, M. W. On the Chemical Diversity of the MAX Phases. *Trends Chem.* **2019**, *1*, 210–233.
- (23) Verger, L.; Natu, V.; Carey, M.; Barsoum, M. W. MXenes: An Introduction of Their Synthesis, Select Properties, and Applications. *Trends Chem.* **2019**, DOI: 10.1016/j.trechm.2019.04.006.
- (24) Natu, V.; Sokol, M.; Verger, L.; Barsoum, M. W. Effect of Edge Charges on Stability and Aggregation of Ti₃C₂T_z MXene Colloidal Suspensions. *J. Phys. Chem. C* **2018**, 122, 27745–27753.
- (25) Lukatskaya, M. R.; Mashtalir, O.; Ren, C. E.; Dall'Agnese, Y.; Rozier, P.; Taberna, P. L.; Naguib, M.; Simon, P.; Barsoum, M. W.; Gogotsi, Y. Cation Intercalation and High Volumetric Capacitance of Two-Dimensional Titanium Carbide. *Science* 2013, 341, 1502–1505.
- (26) Voigt, C. A.; Ghidiu, M.; Natu, V.; Barsoum, M. W. Anion Adsorption, $Ti_3C_2T_z$ MXene Multilayers, and Their Effect on Claylike Swelling. *J. Phys. Chem. C* **2018**, *122*, 23172–23179.
- (27) Ghidiu, M.; Halim, J.; Kota, S.; Bish, D.; Gogotsi, Y.; Barsoum, M. W. Ion-Exchange and Cation Solvation Reactions in Ti₃C₂ MXene. *Chem. Mater.* **2016**, 28, 3507–3514.
- (28) Carey, M.; Hinton, Z.; Sokol, M.; Alvarez, N. J.; Barsoum, M. W. Nylon- $6/\text{Ti}_3\text{C}_2\text{T}_z$ MXene Nanocomposites Synthesized by In Situ Ring Opening Polymerization of ε -Caprolactam and Their Water Transport Properties. ACS Appl. Mater. Interfaces **2019**, 11, 20425—20436.
- (29) Kotsilkova, R.; Petkova, V.; Pelovski, Y. Thermal Analysis of Polymer-Silicate Nanocomposites. *J. Therm. Anal. Calorim.* **2001**, *64*, 591–598.

- (30) Burnside, S. D.; Giannelis, E. P. Synthesis and Properties of New Poly (Dimethylsiloxane) Nanocomposites. *Chem. Mater.* **1995**, 7, 1597–1600.
- (31) Kiliaris, P.; Papaspyrides, C. D. Progress in Polymer Science. *Prog. Polym. Sci.* **2010**, 35 (7), 902–958.
- (32) Hussain, F.; Hojjati, M.; Okamoto, M.; Gorga, R. E. Polymer-Matrix Nanocomposites, Processing, Manufacturing, and Application: An Overview. *J. Compos. Mater.* **2006**, *40*, 1511–1575.
- (33) Mai, Y.-W.; Yu, Z.-Z. Polymer Nanocomposites; Woodhead Publishing, 2006.
- (34) Koo, J. H. *Polymer Nanocomposites*; McGraw-Hill Professional Pub., 2006.
- (35) Gusev, A. A.; Lusti, H. R. Rational Design of Nanocomposites for Barrier Applications. *Adv. Mater.* **2001**, *13*, 1641–1643.
- (36) Verger, L.; Natu, V.; Ghidiu, M.; Barsoum, M. W. Effect of Cationic Exchange on the Hydration and Swelling Behavior of Ti₂C₂T₂ MXenes. *J. Phys. Chem. C* **2019**, *123*, 20044–20050.
- (37) Osti, N. C.; Naguib, M.; Ostadhossein, A.; Xie, Y.; Kent, P. R. C.; Dyatkin, B.; Rother, G.; Heller, W. T.; van Duin, A. C. T.; Gogotsi, Y.; et al. Effect of Metal Ion Intercalation on the Structure of MXene and Water Dynamics on Its Internal Surfaces. ACS Appl. Mater. Interfaces 2016, 8, 8859–8863.
- (38) Becker, O.; Varley, R. J.; Simon, G. P. Thermal Stability and Water Uptake of High Performance Epoxy Layered Silicate Nanocomposites. *Eur. Polym. J.* **2004**, *40*, 187–195.
- (39) Prolongo, S. G.; Gude, M. R.; Urena, A. Water Uptake of Epoxy Composites Reinforced with Carbon Nanofillers. *Composites, Part A* **2012**, *43*, 2169–2175.
- (40) Doyle, M. J.; Maranci, A.; Orowan, E.; Stork, S. T. The Fracture of Glassy Polymers. *Proc. R. Soc. London, Ser. A* **1972**, 329, 137–151.
- (41) McAninch, I. M.; Palmese, G. R.; Lenhart, J. L.; La Scala, J. J. DMA Testing of Epoxy Resins: The Importance of Dimensions. *Polym. Eng. Sci.* **2015**, *55*, 2761–2774.